





## 34 Introduction

35 Pollen is one of the leading causes of allergic diseases worldwide (World Allergy  
36 Organization, 2013), affecting an estimated 15-40 % of the European population (Rojo et  
37 al., 2024). The prevalence of allergic rhinitis and other pollen-related conditions  
38 continues to increase globally (Adams-Groom et al., 2022; Beggs et al., 2023; D'Amato et  
39 al., 2007). The severity of allergic responses depends on several factors, including pollen  
40 concentration, species-specific sensitization thresholds and individual susceptibility  
41 (Rapiejko et al., 2007; Rodríguez-Rajo et al., 2010).

42 In recent decades, climate change has become a key factor influencing the dynamics of  
43 pollen production and dispersion (Anderegg et al., 2021; Lake et al., 2017). Rising  
44 temperatures and elevated atmospheric CO<sub>2</sub> levels contribute to increased pollen  
45 production and cause earlier, longer and more intense pollen seasons for many allergenic  
46 taxa. As a result, exposure periods are becoming more variable and less predictable, with  
47 the timing of peak pollen concentrations often shifting from year to year, which  
48 complicates forecasts of allergy risk (Pacheco et al., 2021; Paudel et al., 2021; Tomczyk  
49 et al., 2025; Ziska et al., 2019).

50 Given these shifts, continuous and precise monitoring of airborne pollen has become  
51 crucial for understanding exposure patterns and supporting public health management,  
52 allergy forecasting and early-warning systems (Grewling et al., 2023; Maya-Manzano et  
53 al., 2023). Pollen monitoring networks were initially established to support allergy  
54 diagnosis and treatment but are now also used to study climate change impacts, track  
55 invasive species and monitor airborne biological particles (Galan et al., 2014)

56 Most monitoring sites still rely on manual sampling methods, such as the Hirst-type  
57 pollen trap (Hirst, 1952), which, despite being standardized and quality-controlled  
58 through aerobiological networks (CEN/TS 16868, 2015), have several limitations. These  
59 include delays of 1-9 days before data are available, low temporal resolution and  
60 uncertainties related to airflow variations, counting methodology, adhesives and  
61 observer differences (Adamov et al., 2021; Trivino et al., 2023). However, Hirst-type traps  
62 remain the reference against which other pollen and fungal spore detection methods are  
63 evaluated (Tummon et al., 2021).

64 In recent years, technological advances have enabled real-time detection of pollen and  
65 other bioaerosols, using diverse approaches and instruments (Buters et al., 2024; Maya-  
66 Manzano et al., 2023). These systems allow continuous monitoring, higher temporal  
67 resolution and improved responsiveness for public health and research applications. The  
68 rapid evolution of these technologies is transforming pollen monitoring, providing critical  
69 real-time information for allergy management, climate studies and environmental  
70 research (Sauvageat et al., 2020). One of the devices is the Swisens Poleno Jupiter, an  
71 advanced instrument designed for real-time bioaerosol monitoring, capable of detecting  
72 and identifying airborne particles such as pollen. It combines digital holography with



73 fluorescence measurements, providing detailed information on both the morphology and  
74 composition of particles to support the development of automatic pollen detection  
75 systems (Erb et al., 2025). The recent studies highlight that automatic pollen detections,  
76 even with advanced machine learning, has not achieved full accuracy or maturity and  
77 further work is needed to generalize such models across more pollen species and  
78 conditions. They emphasize that significant improvements in algorithms, training data and  
79 validations strategies are still required before automated pollen identification can match  
80 expert human analysis (Faroq et al., 2025; Gimenez et al., 2024; Shamrat et al., 2024). We  
81 have undertaken some of these gaps by the extending and refining the reference pollen  
82 database for the Swisens Poleno Jupiter automatic monitoring system.

83 For this purpose, during the pollination seasons, local pollen samples were collected and  
84 used to retrain the neural network model. We hypothesised that the retrained model  
85 would provide more accurate and timely predictions of airborne pollen concentrations  
86 compared to models trained solely on foreign datasets. The study describes the  
87 measurement campaigns carried out as part of the development of automatic pollen  
88 detection methods. To date, there are no studies explicitly emphasizing the importance  
89 of retraining neural network models using locally collected pollen datasets that reflect  
90 real environmental conditions. Secondly, we analysed the similarities and differences in  
91 the diurnal concentration patterns of five pollen taxa — *Alnus* (alder), *Betula* (birch),  
92 *Fraxinus* (ash), *Pinus* (pine) and *Quercus* (oak). These tree species are known for their  
93 allergenic potential, particularly *Alnus* and *Betula* from the Betulaceae family  
94 (Biedermann et al., 2019). Owing to their high pollen productivity, airborne concentrations  
95 of these taxa can fluctuate substantially (Malkiewicz et al., 2016). We hypothesised that  
96 diurnal variability would show comparable patterns among taxa with similar pollen  
97 release mechanisms, while differing among species with distinct phenological or  
98 aerodynamic characteristics. Additionally, the availability of high-resolution hourly data  
99 enabled us to assess the influence of meteorological conditions on short-term variability  
100 in pollen concentrations. We used standard meteorological parameters, including  
101 temperature, relative humidity, precipitation, wind and sunshine duration, to obtain a  
102 comprehensive understanding of the factors influencing pollen concentrations. However,  
103 in order to obtain a broad view of the factors influencing pollen concentrations, we also  
104 included the planetary boundary layer height among the analysed parameters. Although  
105 frequently mentioned in aerobiology, its influence on hourly pollen variability has rarely  
106 been investigated compared to standard local meteorological drivers.

107 This study provides two years analysis of diurnal airborne pollen dynamics using data  
108 from an automatic real-time monitoring system. It is the first to employ the Swisens  
109 Poleno Jupiter detector for continuous, high-resolution assessment of diurnal variability  
110 across multiple pollen seasons. In contrast to previous studies based on traditional Hirst-  
111 type volumetric traps (Clot, 2001; Kämpylä, 1984; Kasprzyk et al., 2001; Ščevková et al.,



112 2015), this approach allows for a more detailed and consistent evaluation of hourly  
113 fluctuations and interannual trends in pollen concentrations.

## 114 2. Data and methods

### 115 2.1 Automatic detection

#### 116 Location and time frame

117 The detector Swisens Poleno Jupiter is installed in Wrocław (southwestern Poland), on  
118 the roof of the Department of Climatology and Atmosphere Protection, University of  
119 Wrocław, at an elevation of 20 meters above ground level. The instrument is co-located  
120 with a standard Hirst-type volumetric trap, allowing for direct comparison between  
121 automatic and manual monitoring methods. The measurements cover the periods of  
122 2024 and 2025, encompassing two complete pollen seasons.

123



124

125

126 Figure 1. Location of the Swisens Poleno Jupiter detector in Wrocław, Poland (red dot); the  
127 inset shows the location of Poland within Europe. The European map is based on Natural  
128 Earth data, while the city map uses data from OpenStreetMap contributors.

129

130



131 Description of the detector

132 The Swisens Poleno Jupiter (Swisens AG) is an airborne cytometer designed for real-time  
133 analysis of individual particles ranging from 0.5 to 300  $\mu\text{m}$ , operating at a sampling flow  
134 rate of 40 liters per minute. As particles pass through the instrument, they are  
135 concentrated within the measurement chamber, where two orthogonally positioned  
136 lasers detect each particle, providing estimates of size and velocity based on light  
137 scattering. Once detected, the particle is captured by two greyscale holographic cameras  
138 positioned at 90° angles to each other and perpendicular to the airflow. The holographic  
139 images are reconstructed numerically to a resolution of 200  $\times$  200 pixels, with each pixel  
140 representing 0.595  $\times$  0.595  $\mu\text{m}$  in the physical domain. These images enable precise  
141 characterization of particle morphology. Immediately after imaging, laser-induced  
142 fluorescence (LIF) is measured. Particles are sequentially excited by three laser sources  
143 (280, 365 and 405 nm) and the resulting fluorescence is recorded across five spectral  
144 channels (333-381, 411-459, 465-501, 539-585 and 658-694 nm), hereafter referred to by  
145 their central wavelengths: 357, 435, 483, 562 and 676 nm. Fluorescence emission is  
146 captured by silicon photomultipliers (SiPMs), producing up to 15 intensity measurements  
147 per particle. Due to saturation and single-photon excitation effects, the effective number  
148 of usable fluorescence channels is 13. The fluorescence data undergo additional  
149 preprocessing to enhance usability and robustness. In this work, analysis focuses on  
150 particle morphology (from holographic images) and chemical composition (from  
151 fluorescence intensities). The instrument also performs polarized-scattered-light  
152 measurements, which are not used here (Erb et al., 2024; Erb et al., 2025; Sauvageat et  
153 al., 2020).

154

155 Measurement campaigns

156 The measurement campaigns were designed to collect high-quality reference data for  
157 retraining and validating the automatic pollen detection model. A total of five taxa- *Alnus*,  
158 *Betula*, *Fraxinus*, *Quercus* and *Pinus* - were included in the experiments, with the number  
159 of campaigns, recorded events, measurement duration and amount of pollen adjusted to  
160 the availability and characteristics of each species (see Table 1). The total number of  
161 recorded events ranged from 3 622 for *Fraxinus* to 7 233 for *Betula*, with measurement  
162 durations between 19 min and 68 min and pollen quantities from 0.5 ml to 1.25 ml.

163 Each campaign consisted of a series of controlled laboratory experiments aimed at  
164 introducing locally collected pollen into the automatic detector under standardized  
165 conditions. The main goal was to extend the pollen database with accurately identified  
166 local taxa and to ensure the consistency and reliability of data used for model  
167 development.



168 The campaigns were carried out using the Swisens Poleno Atomizer, a device that enables  
169 controlled aerosolization of pollen grains directly from a test tube into the Swisens Poleno  
170 Jupiter detector. Swisens Atomizer delivers the particles directly to the Swisens Poleno  
171 detector under controlled conditions. This system disperses selected particles at a stable  
172 rate by combining vibration and airflow. The vibration frequency, amplitude and blower  
173 speed can be precisely adjusted. The Swisens Atomizer is positioned directly above the  
174 Swisens Poleno Jupiter so that the sampled air contains the target pollen particles. This  
175 setup allows simultaneous measurement and labeling of all collected data with the  
176 corresponding particle type (Erb et al., 2025). The entire process is managed via an  
177 integrated computer system, which provides feedback on instrument performance and  
178 enables data recording when the conditions are optimal.

179 Each campaign followed a structured workflow:

- 180 1. Pollen preparation - Inflorescences of *Alnus*, *Betula*, *Fraxinus*, *Quercus* and *Pinus*  
181 were collected during their natural pollination periods and processed to obtain  
182 clean pollen grains. It is important to monitor meteorological conditions and  
183 collect catkins when they open naturally (during sunny weather and temperatures  
184 above 10 °C) or to collect inflorescences and let them open in warm, dry  
185 conditions.
- 186 2. Measurement phase - The Atomizer introduced the pollen into the detector, with  
187 continuous monitoring to ensure high-quality data.
- 188 3. Data validation and selection - Collected signals were reviewed to remove artifacts  
189 or non-pollen particles.
- 190 4. Dataset compilation - Verified data were organized using *Swisens Data Explorer*  
191 software, forming the basis for neural network retraining.
- 192 5. Model retraining and testing - The new model was trained on a subset of the  
193 dataset and evaluated on an independent portion to assess detection  
194 performance.

195 The campaigns were repeated for each taxon to ensure representative coverage of the  
196 dominant allergenic species in the region. Each dataset contained thousands of  
197 individual particle measurements, reflecting both the natural variability of pollen  
198 availability and the specific conditions of each measurement session.

199

200

201

202



203

Table 1. Summary of total dataset sizes for each pollen taxon

Taxa	Total number of recorded events	Number of campaigns	Duration of the measurement phases	Amount of pollen per campaigning
<i>Alnus</i>	6 409	5	50 min	1.25 ml
<i>Betula</i>	7 233	2	68 min	1.25 ml
<i>Fraxinus</i>	3 622	1	19 min	0.5 ml
<i>Quercus</i>	5 975	2	52 min	1 ml
<i>Pinus</i>	6 572	1	45 min	1 ml

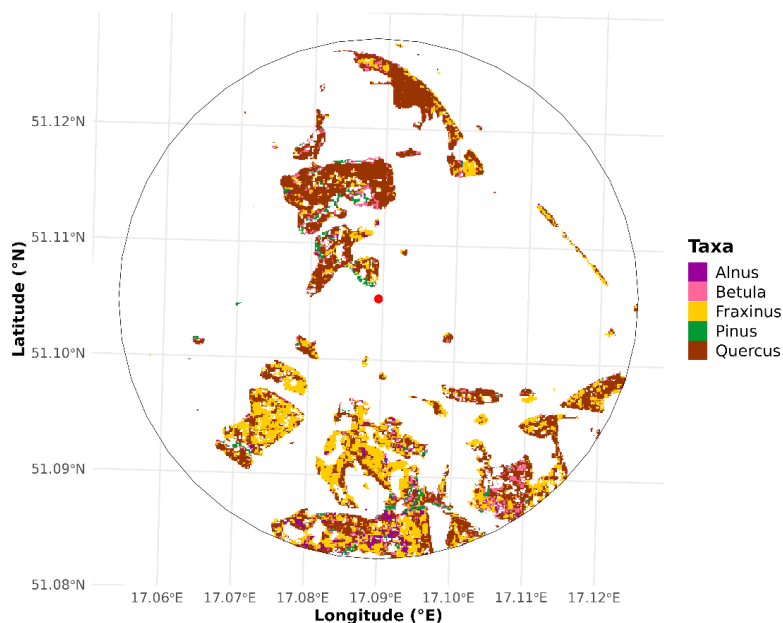
204

205 For reliable particle identification, input data must contain only the target pollen type.  
206 Environmental samples often include unwanted particles such as dust, other pollen, or  
207 plant debris, necessitating a data cleaning step. Using the SwisensDataExplorer tool,  
208 expert annotators manually removed non-target particles, producing “clean” datasets for  
209 training. Typical exclusions included double particles, irregular shapes and out-of-range  
210 sizes, while blurred images were retained to preserve natural variability. Although manual  
211 cleaning is subjective and not an absolute ground truth, it ensures that essential particle  
212 characteristics are maintained. These cleaned datasets were then used to retrain a neural  
213 network and provide a new detection model.

214

215 2.2. Station surroundings

216



217

218 Figure 2. Station surroundings based on data from Grabska-Szwagrzyk et al. (2024); map  
219 prepared by the author.

220

221 Within a 2.5 km buffer around the monitoring station, the analyzed tree species are  
222 predominantly located to the north and south of the site. The northern area,  
223 corresponding to Park Szczytnicki, is mainly dominated by *Quercus*, *Pinus* and *Betula*. In  
224 contrast, the southern sector, located near the Odra River, contains the highest density of  
225 trees, particularly *Fraxinus* and *Quercus*, with additional occurrences of *Betula* and *Alnus*  
226 along the riverbanks. The western and eastern directions are sparsely vegetated,  
227 containing only isolated individual trees rather than larger clusters.

228 2.3. Hirst trap measurements

229 For validation purposes, airborne pollen samples were collected using a volumetric 7-day  
230 Hirst-type trap (Hirst, 1952), co-located with the Swisens Poleno detector at the same  
231 height on the roof of the Institute of Climatology and Atmospheric Protection. The Hirst  
232 trap continuously draws in air and pollen grains, along with other particles, adhere to a  
233 prepared sticky tape. After one week, the tape is replaced and laboratory slides are  
234 prepared, from which pollen grains are counted following European standards (Galán et  
235 al., 2014), i.e., from four continuous horizontal bands. These Hirst-type measurements  
236 served as reference data to validate the results obtained from the Swisens Poleno  
237 instrument and the neural network model.

238



239 2.5. Meteorological data

240 Meteorological data were obtained from automatic measurements at the Department of  
241 Climatology and Atmospheric Protection, where the detector and Hirst pollen trap are  
242 located. The dataset includes mean hourly records of temperature at 2m [°C], wind speed  
243 [m/s] and direction [°] at 10m, relative humidity at 2m [%], sum of precipitation [mm] and  
244 sunshine duration [hours]. Additionally, the WRF model was used to determine the hourly  
245 variability of planetary boundary layer (PBL) height [m]; however, only data for 2024 are  
246 presented, as simulations for the current year are still ongoing.

247 2.6. Method of analysis

248 Evaluation of the old and new model results

249 The pollen season was determined separately for both the automatic real-time detector  
250 (Swisens Poleno Jupiter) and the reference Hirst-type sampler using the 90% method  
251 (Nilsson and Persson, 1981). The start of the pollen season was defined as the day when  
252 the cumulative pollen count exceeded 5% of the annual total and the end as the day when  
253 it surpassed 95%. These season limits were then applied consistently for validation of the  
254 automatic measurements and for the subsequent statistical and diurnal variability  
255 analyses.

256 To evaluate temporal consistency, daily concentrations from two consecutive pollen  
257 seasons were compared for both the old and new automatic models against Hirst  
258 reference data. The baseline model was originally developed by MeteoSwiss and trained  
259 on datasets obtained from the MeteoSwiss pollen monitoring network in Switzerland. The  
260 official GitHub repository provides access to the MCH 2022 model (MeteoSwiss, 2022).  
261 The current model was retrained using locally collected pollen data from Wrocław,  
262 Poland, for the same taxa, with the aim of improving predictive performance under local  
263 environmental conditions. While the previous model relied solely on holographic images,  
264 the new model incorporates both holography and fluorescence spectral information.  
265 Cruozy et al. (2025) demonstrated that including additional information improves  
266 detection performance; however, studies on the use of locally collected pollen to improve  
267 model performance for specific taxa remain scarce, which is the primary focus of the  
268 present work.

269 Agreement between the automatic method and the Hirst was quantified using the  
270 coefficient of determination ( $R^2$ ) and the root mean square error (RMSE).  $R^2$  assessed the  
271 proportion of variance explained, while RMSE provided an absolute measure of average  
272 daily deviation.

273 For evaluation by exposure level, hourly concentrations were binned into four classes  
274 (low, medium, high, very high). Thresholds were defined individually per taxon based on  
275 observed distributions. As an example, *Betula* (birch) classes were:



276 Low:  $\leq 30$  pollen grains  $m^{-3}$

277 Medium: 31-80 pollen grains  $m^{-3}$

278 High: 81-150 pollen grains  $m^{-3}$

279 Very high:  $> 150$  pollen grains  $m^{-3}$

280 (Analogous taxon-specific thresholds were applied for *Alnus*, *Fraxinus*, *Pinus* and  
281 *Quercus*.)

282 Model outputs (old vs. new) were evaluated for each taxon and concentration class using  
283 contingency and skill metrics computed from counts of True Positives (TP), False Positives  
284 (FP) and False Negatives (FN). Derived metrics included: Probability of Detection (POD =  
285  $TP/(TP+FN)$ ), False Alarm Ratio (FAR =  $FP/(TP+FP)$ ), Critical Success Index (CSI =  
286  $TP/(TP+FP+FN)$ ) and Success Rate (SR =  $(TP+TN)/total$ , where TN is True Negatives). These  
287 metrics were reported separately for each taxon and concentration level to characterize  
288 model behavior across exposure ranges.

289

290 Diurnal variability of pollen concentrations

291 Hourly concentrations from the Swisens Poleno Jupiter (new model) were analyzed to  
292 characterize diurnal patterns for each taxon. All timestamps were recorded in  
293 Coordinated Universal Time (UTC). Differences in hourly distributions between the two  
294 seasons were quantified and visualized to identify peak exposure hours.

295 Diurnal variability of meteorological parameters and pollen data

296 Finally, an overall correlation matrix was constructed to assess the relationships between  
297 hourly meteorological variables (temperature, wind speed and direction, relative  
298 humidity, precipitation and sunshine duration) and pollen concentrations obtained from  
299 the Swisens Polleno Jupiter (new model). Subsequently, for each taxon, Spearman rank  
300 correlations were calculated between pollen concentration and each meteorological  
301 variable separately for each month within the respective flowering season, in order to  
302 capture the seasonal and hourly variability of these relationships. Previous research has  
303 shown that meteorological conditions strongly influence airborne pollen concentrations  
304 (Dąbrowska-Zapart et al., 2020; Kluska et al., 2020; Malkiewicz et al., 2016; Tomczyk et  
305 al., 2025), justifying the use of correlation analyses to assess their effect on hourly pollen  
306 variability. Statistical significance was assessed at three levels ( $p < 0.05$ ,  $p < 0.01$  and  $p <$   
307  $0.001$ ) and correlation magnitudes and significance patterns were reported and mapped  
308 to hourly contexts.

309 The hourly planetary boundary layer (PBL) height was determined using the WRF  
310 numerical meteorological model, with model setup and parameterizations following  
311 Skamarock et al. (2021). Spearman's rank correlations were then calculated between PBL



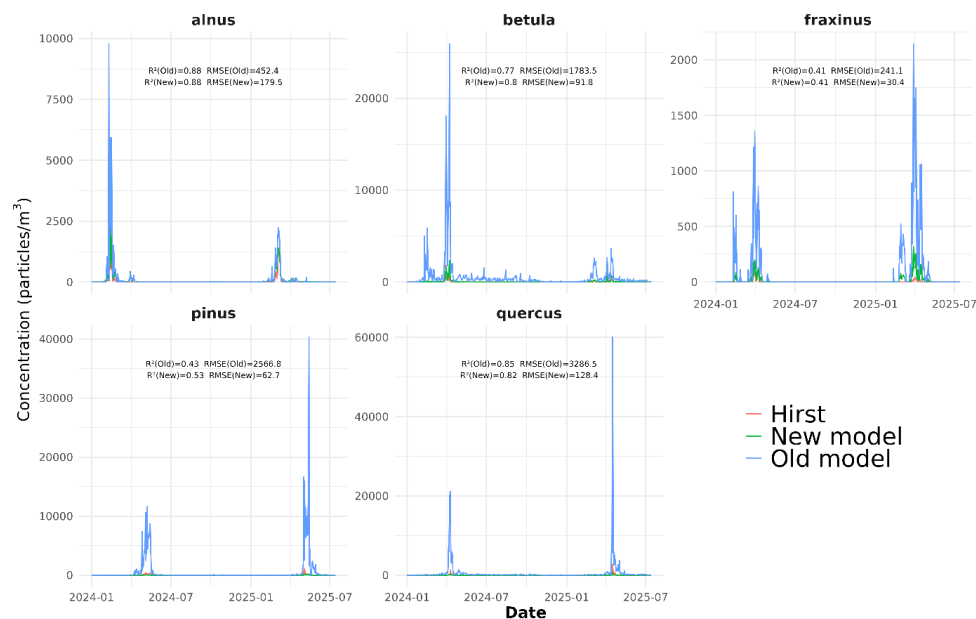
312 height and pollen concentrations to assess how boundary layer dynamics influence  
313 short-term variations in airborne pollen levels. Correlations for all variables were adjusted  
314 for multiple comparisons using the Bonferroni correction to account for the large number  
315 of observations.

316 A wind-rose analysis was performed using concurrent hourly wind direction and speed  
317 records to identify prevailing wind sectors associated with the highest pollen  
318 concentrations. These wind sector concentration patterns were compared spatially with  
319 land-cover/land-use maps (see Figure 2) to infer potential source areas and directional  
320 contributions to measured pollen loads. Figure 2 was created based on detailed tree  
321 distribution maps developed by Grabska-Szwagrzyk (2024), who classified 16 dominant  
322 tree species and genera across Poland using time series of Sentinel-2 imagery.

### 323 3. Results

#### 324 3.1 Pollen concentrations from the Swisens Polleno Jupiter and Hirst

325 This presents a comparison between the machine learning model trained on Swiss pollen  
326 data (old model) and the newly retrained model using local taxa (new model) against Hirst  
327 measurements, highlighting differences in predicted concentrations, temporal patterns  
328 and deviations from observed values.



329

330 Figure 3. Daily pollen concentrations from old and new ML models compared with Hirst  
331 reference data.

332



333 For *Alnus* and *Betula*, both models capture the main seasonal peaks well, with *Alnus*  
334 showing a pronounced early spring maximum. The new model closely follows the Hirst  
335 observations in both shape and timing of peaks, while the old model tends to  
336 overestimate concentrations. For *Alnus*, both models achieve the same  $R^2 = 0.88$ , but  
337 the new model shows a much lower RMSE (179.5 vs 452.4, for old and new model  
338 respectively - here and thereafter), indicating improved accuracy. Similarly, for *Betula*, the  
339 new model slightly improves the determination coefficient ( $R^2 = 0.80$  vs 0.77) and  
340 reduces RMSE substantially (91.8 vs 1783.5).

341 For *Fraxinus*, concentrations remain relatively low, with both models capturing the timing  
342 of peaks. The new model performs markedly better, maintaining the same  $R^2 = 0.41$  but  
343 achieving a much lower RMSE (30.4 vs 241.1), reflecting greater precision in reproducing  
344 small variations.

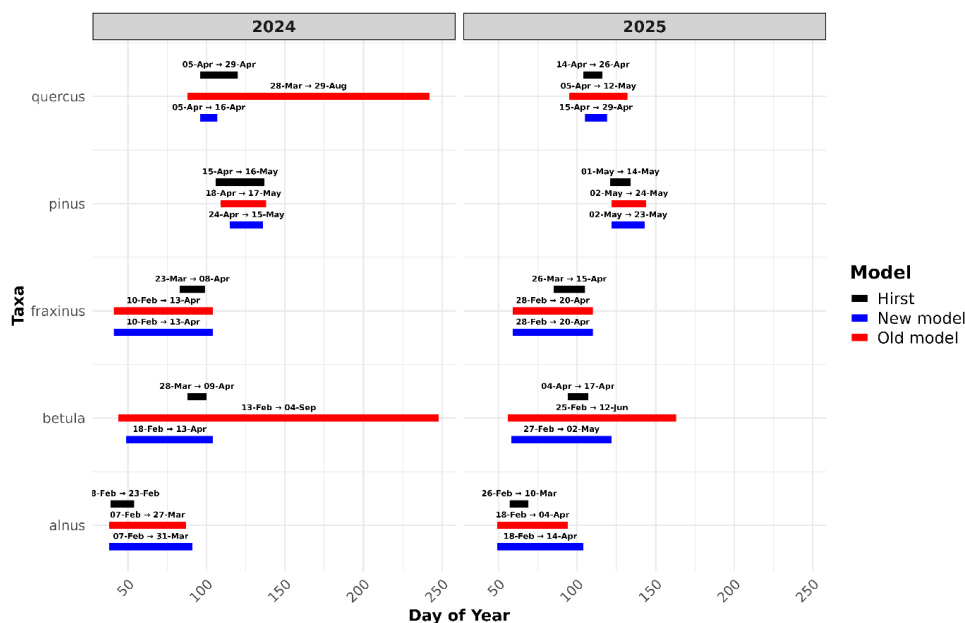
345 In the case of *Pinus*, the new model better reproduces both low and moderate  
346 concentration periods, while the old model significantly overestimates peak magnitudes.  
347 This improvement is confirmed by a higher  $R^2$  (0.53 vs 0.43) and a significantly reduced  
348 RMSE (62.7 vs 2566.8).

349 For *Quercus*, a distinct late spring peak is observed. Both models correctly identify the  
350 timing of high pollen events, but the new model more accurately represents the peak  
351 structure and intensity, with a slightly lower  $R^2$  (0.82 vs 0.85) and a drastically smaller  
352 RMSE (128.4 vs 3286.5), highlighting a much-improved fit to observed concentrations.

353

### 354 **3.2 Comparison of Models - Pollen Season Duration**

355 This examines how each model predicts the start and end of the pollen season, analyzing  
356 differences in season length and timing in comparison with observed data.



357

358

359 Figure 4. Start and end dates of pollen seasons for the studied taxa.

360

361 For *Alnus*, both years show that the new model reproduces the Hirst-derived start dates  
 362 well, whereas the end dates are captured less accurately (2024: 7 Feb-27 Mar vs 8 Feb-  
 363 23 Feb; 2025: 18 Feb-4 Apr vs 26 Feb-10 Mar), while the old model predicts a longer  
 364 season (until the end of March or mid-April).

365 For *Betula*, the old model largely overestimates the pollen season duration (2024: 13 Feb-  
 366 4 Sep; 2025: 25 Feb-12 Jun), while the new model (2024: 18 Feb-13 Apr; 2025: 27 Feb-2  
 367 May) better captures the Hirst timing (2024: 28 Mar-9 Apr; 2025: 4 Apr-17 Apr).

368 For *Fraxinus*, both models identify the onset of the season earlier than Hirst in 2024 (10  
 369 Feb-13 Apr vs 23 Mar-8 Apr), but the new model better reproduces the duration. A similar  
 370 pattern appears in 2025, where the new model (28 Feb-20 Apr) aligns with Hirst (26 Mar-  
 371 15 Apr) more accurately than the old model, which extends the season.

372 For *Pinus*, both models capture the general spring timing, but the new model aligns more  
 373 closely with observations (2024: 18 Apr-17 May vs 15 Apr-16 May; 2025: 2 May-23 May vs  
 374 1 May-14 May), while the old model slightly underestimates the duration.

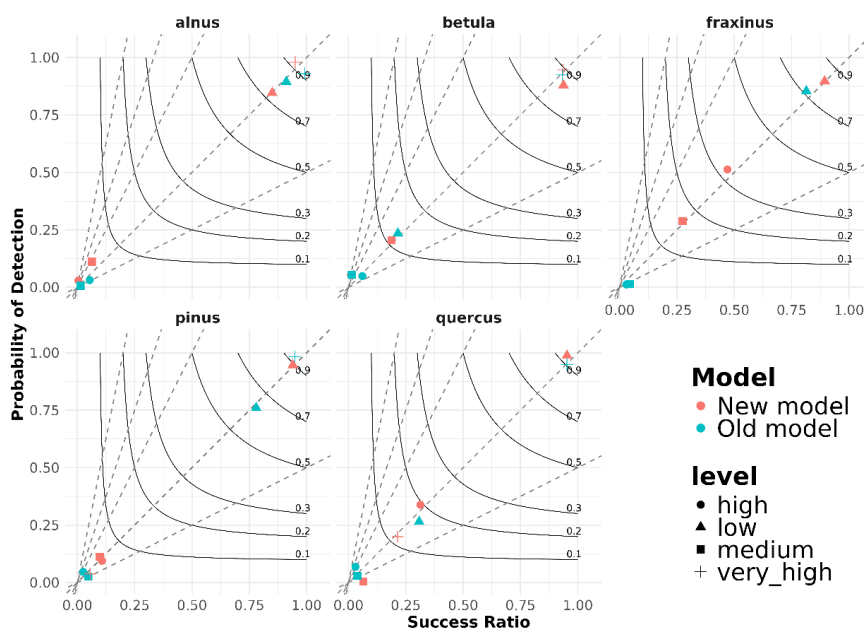
375 For *Quercus*, the new model accurately reproduces the observed periods (2024: 5 Apr-16  
 376 Apr vs 5 Apr-29 Apr; 2025: 15 Apr-29 Apr vs 14 Apr-26 Apr), whereas the old model



377 significantly extends the season (2024: 28 Mar-29 Aug; 2025: 5 Apr-12 May), indicating  
378 overprediction of long-term pollen presence.

### 379 3.3 Comparison of Models - Performance Diagram

380 Model performance is evaluated using metrics such as accuracy, precision, recall and F1-  
381 score. Performance diagrams and statistical analyses are provided to illustrate model  
382 strengths and weaknesses.



383

384

385 Figure 5. Performance of automatic ML models compared with Hirst reference data.

386

387 Detection of *Alnus* pollen remained challenging for both models at medium and high  
388 concentrations, resulting in low POD (<0.25) and success ratios below 0.2. The new  
389 model shows noticeable improvement at low concentrations (POD  $\approx$  0.75, SR  $\approx$  0.7),  
390 indicating better sensitivity to early pollen occurrence, while both models perform  
391 perfectly at very high concentrations (POD  $\approx$  1.0, SR  $\approx$  1.0), confirming reliability during  
392 peak events.

393 For *Betula*, the new model clearly outperforms the old one at low concentrations (POD  $\approx$   
394 0.9 vs 0.6; SR  $\approx$  0.8 vs 0.6), while maintaining similar performance at higher levels (POD  $\approx$   
395 1.0, SR  $\approx$  1.0). Detection at medium levels remains limited for both models, though the  
396 new model achieves higher accuracy and fewer false alarms overall.



397 For *Fraxinus*, improvements are mainly visible at medium and high concentrations (old  
398 model:  $POD \approx 0.1$ ,  $SR \approx 0.1$ ; new model: medium 0.3, 0.3 and high 0.5, 0.5), reflecting  
399 better seasonal detection capability. Very high concentrations are successfully detected  
400 by both models ( $POD \approx 1.0$ ,  $SR \approx 1.0$ ), while at low concentrations the new model shows  
401 moderate improvement over the old model.

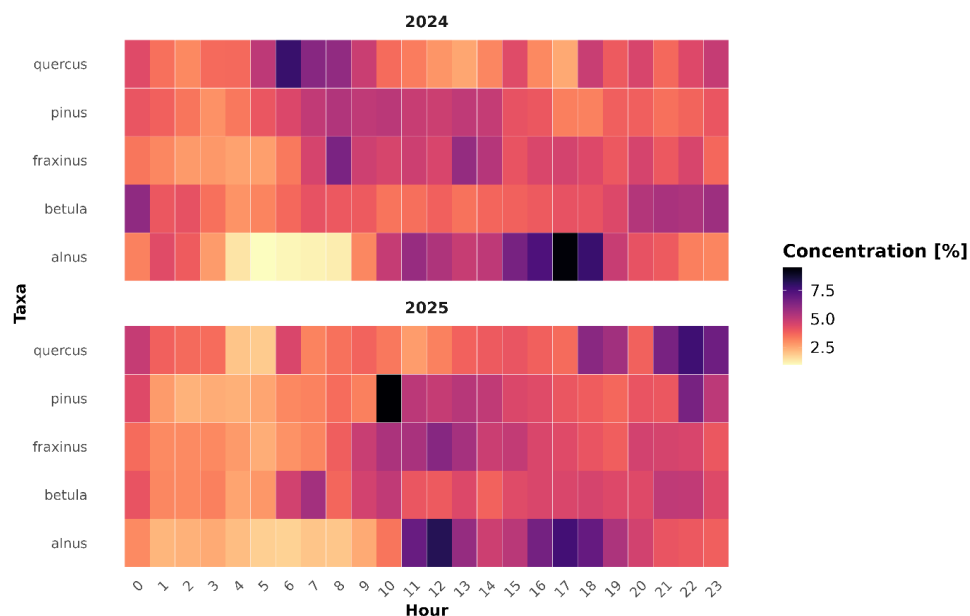
402 In the case of *Pinus*, the new model achieves strong detection performance at low  
403 concentrations ( $POD \approx 0.95$ ,  $SR \approx 0.9$ ), outperforming the old model ( $POD \approx 0.7$ ,  $SR \approx 0.6$ ).  
404 Both models detect very high concentrations perfectly ( $POD \approx 1.0$ ,  $SR \approx 1.0$ ), though  
405 detection at medium and high levels remains less reliable.

406 For *Quercus*, the new model substantially improves detection at low concentrations ( $POD$   
407  $\approx 0.97$ ,  $SR \approx 0.9$ ), outperforming the old model. Detection at medium concentrations  
408 remains very low ( $POD \approx 0.1$ ,  $SR \approx 0.1$ ), while at high concentrations the new model  
409 performs better than the old one. Very high concentrations are better detected by the old  
410 model.

411

#### 412 3.4 Hourly Concentration Patterns over Two Years

413 Hourly Swisens Polleno Jupiter (the new model) pollen concentration profiles for two  
414 consecutive years are presented, showing diurnal trends, seasonal variations and year-  
415 to-year differences.



416

417 Figure 6. Hourly pollen profiles from the Swisens Poleno Jupiter for two consecutive years.



418

419 For *Alnus*, the highest contributions to the seasonal pollen load were consistently  
420 observed during the late afternoon hours, specifically between 16:00 and 18:00. In 2024,  
421 hourly contributions for 16:00, 17:00 and 18:00 reached 9.5%, 8% and 5% of the total  
422 seasonal load, while in 2025 they were slightly lower but still substantial, at 7.5%, 7% and  
423 5%, respectively. This pattern reflects a typical daily trend, with the lowest pollen  
424 concentrations in the morning, higher levels around midday and a peak in the late  
425 afternoon, highlighting this period as critical for *Alnus* pollen dispersal and its overall  
426 impact on seasonal exposure.

427 *Betula* displayed a distinct temporal pattern, with peak pollen concentrations occurring  
428 in the evening between 20:00 and 00:00, as well as in the morning between 06:00 and  
429 10:00. During these periods, hourly contributions ranged from 4% to 5% of the seasonal  
430 total, indicating that both morning and evening represent windows of elevated *Betula*  
431 pollen concentrations, with potential implications for allergy sufferers during these times.

432 For *Fraxinus*, pollen concentrations gradually increased in the morning, reaching a peak  
433 around midday (11:00–14:00), with hourly contributions ranging from 5% to 6%.  
434 Additional moderate peaks were observed in the late morning, early afternoon and  
435 evening, reflecting a more extended period of pollen availability compared to *Alnus* and  
436 *Betula*. This pattern suggests that *Fraxinus* contributes to sustained exposure throughout  
437 the central part of the day.

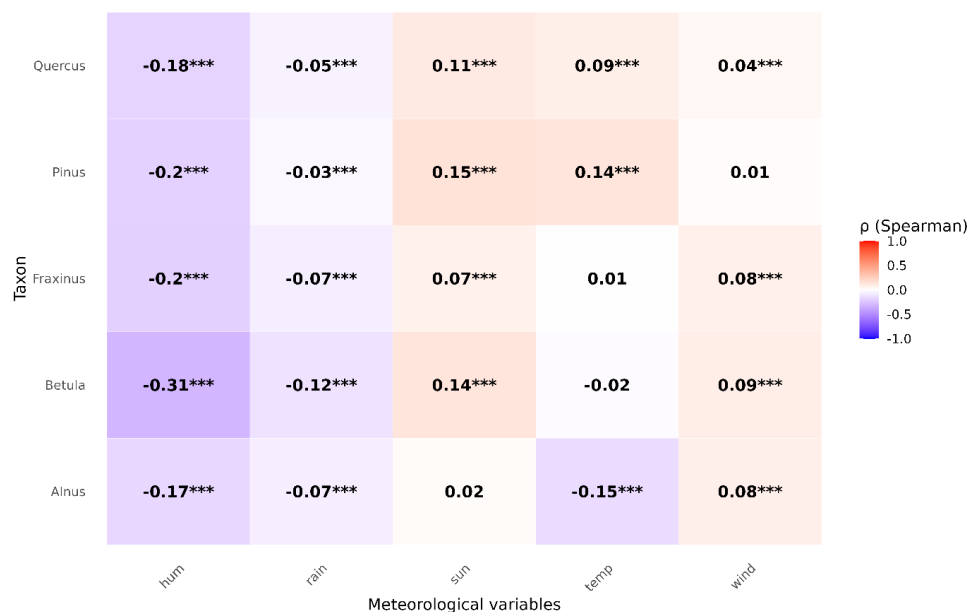
438 *Pinus* exhibited pronounced morning and midday peaks, with the highest hourly  
439 contribution reaching 10% at 10:00 in 2025. Overall, pollen levels remained consistently  
440 elevated throughout the day, ranging from 3% to 6%, with the lowest values observed  
441 between 03:00 and 05:00. This extended period of substantial emission reflects both high  
442 variability and prolonged daytime dispersal, making *Pinus* a major contributor to airborne  
443 pollen over a broad temporal window.

444 *Quercus* exhibited a bimodal pattern of pollen concentrations, with morning peaks  
445 occurring between 06:00 and 09:00 and a second, more pronounced peak in the evening  
446 between 18:00 and 00:00. Hourly contributions during these periods reached up to 8% of  
447 the seasonal load, indicating that both early morning and evening represent critical  
448 windows for *Quercus* pollen exposure.

449

### 450 **3.5 Meteorological Parameters and Pollen Concentrations**

451 The Spearman correlation matrix (Fig. 7) provides an overview of the associations  
452 between hourly meteorological parameters and pollen concentrations for multiple tree  
453 taxa, thereby identifying the principal drivers of pollen variability and informing their  
454 predictive potential.



455

456 Figure 7. Overall Spearman correlation matrix between meteorological variables and  
457 pollen concentrations.

458

459 In the case of *Alnus*, pollen concentration showed a clear negative correlation with  
460 relative humidity ( $\rho = -0.17$ ,  $p < 0.001$ ) and temperature ( $\rho = -0.15$ ,  $p < 0.001$ ). In contrast,  
461 the influence of wind and sunshine duration was relatively weak ( $\rho = 0.08$  and  $0.02$ ,  
462 respectively).

463 *Betula* exhibited the strongest negative correlation with relative humidity ( $\rho = -0.12$ ,  $p <$   
464  $0.001$ ), whereas the effect of temperature was minimal ( $\rho = -0.02$ , ns) and solar radiation  
465 showed a moderately positive effect ( $\rho = 0.14$ ,  $p < 0.001$ ).

466 For *Fraxinus*, pollen concentration correlated moderately positively with sunshine  
467 duration ( $\rho = 0.07$ ,  $p < 0.001$ ) and wind ( $\rho = 0.08$ ,  $p < 0.001$ ), while humidity ( $\rho = -0.07$ ,  $p <$   
468  $0.001$ ) and temperature ( $\rho = -0.20$ ,  $p < 0.001$ ) had weaker negative effects.

469 *Pinus* showed the highest positive correlations with sunshine duration ( $\rho = 0.15$ ,  $p < 0.001$ )  
470 and temperature ( $\rho = 0.14$ ,  $p < 0.001$ ), whereas humidity had a slight negative influence ( $\rho$   
471  $= -0.03$ ,  $p < 0.001$ ) and wind was nearly neutral ( $\rho = 0.01$ , ns).

472 In the case of *Quercus*, pollen exhibited a moderate positive relationship with  
473 temperature ( $\rho = 0.09$ ,  $p < 0.001$ ) and weaker positive correlations with sunshine duration  
474 ( $\rho = 0.11$ ,  $p < 0.001$ ) and wind ( $\rho = 0.04$ ,  $p < 0.001$ ), while humidity showed a slight negative  
475 effect ( $\rho = -0.05$ ,  $p < 0.001$ ).



476 The following analysis (Fig. 1S) focuses on the hourly correlations between these  
477 variables, highlighting how their relationships change throughout the day.

478

479 Figure 1S. Hourly Spearman correlation matrix between meteorological variables and  
480 *Alnus* pollen concentrations.

481 Figure 2S. Hourly Spearman correlation matrix between meteorological variables and  
482 *Betula* pollen concentrations.

483 Figure 3S. Hourly Spearman correlation matrix between meteorological variables and  
484 *Fraxinus* pollen concentrations.

485 Figure 4S. Hourly Spearman correlation matrix between meteorological variables and  
486 *Pinus* pollen concentrations.

487 Figure 5S. Hourly Spearman correlation matrix between meteorological variables and  
488 *Quercus* pollen concentrations.

489

490 For *Alnus*, the Spearman results indicate a clear diurnal/seasonal pattern. The  
491 air temperature, in the pollen season, shows a strong positive correlation with pollen  
492 counts, particularly during midday-afternoon. Relative humidity is negatively correlated  
493 with pollen counts. The signal is the strongest in March, in early morning hours (around  
494 08:00) and night/late-evening (19-21:00). When comparing February and March,  
495 temperature emerges as the dominant driver in February, while in March humidity  
496 becomes the most influential meteorological factor shaping pollen concentrations.

497 For *Betula*, Spearman correlations revealed strong positive associations between pollen  
498 concentrations and air temperature, particularly during daytime hours, with peak  
499 correlations reaching  $r \approx 0.65-0.70$  ( $p < 0.01$ ). Relative humidity was consistently  
500 negatively correlated ( $r \approx -0.45$  to  $-0.60$ ,  $p < 0.05-0.01$ ), while sunshine duration showed  
501 moderate positive effects in the morning. Rainfall effects were mostly non-significant.  
502 Seasonal differences indicated that in March, temperature and humidity effects were  
503 concentrated during the day, whereas in April, their influence extended more evenly into  
504 the evening and night, with wind becoming a more important factor.

505 For *Fraxinus*, air temperature positively influenced pollen concentrations, with  
506 correlations reaching  $r \approx 0.60-0.68$  ( $p < 0.01$ ), particularly during daytime hours in March  
507 and during the afternoon, evening and night in April. Relative humidity showed a negative  
508 relationship ( $r \approx -0.40$  to  $-0.55$ ,  $p < 0.05-0.01$ ), especially in the early and late hours of  
509 March and during the night in April. Sunshine duration, rainfall and wind effects were  
510 generally non-significant.



511 For *Pinus*, temperature effects were weaker compared to other taxa, showing moderate  
512 negative correlations during early morning and late-night hours in May ( $r \approx -0.30$  to  $-0.40$ ,  
513  $p < 0.05$ ). Relative humidity consistently exhibited strong negative correlations ( $r \approx -0.50$   
514 to  $-0.65$ ,  $p < 0.01$ ), particularly in May, while sunshine duration showed occasional  
515 positive associations during the afternoon. Wind and rainfall effects were negligible.

516 For *Quercus*, pollen concentrations showed strong positive correlations with air  
517 temperature throughout the entire day in April ( $r \approx 0.60$ – $0.72$ ,  $p < 0.01$ ), while other  
518 meteorological factors had no significant influence.

519

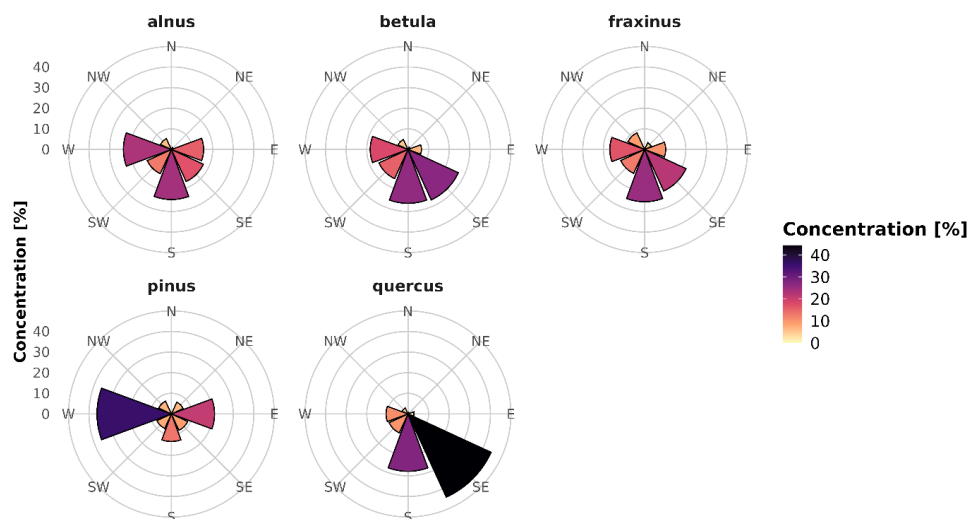
520 Table 2. Spearman’s correlations between hourly pollen concentrations and PBL height  
521 in Wrocław (2024–2025).

Taxa	<i>Alnus</i>	<i>Betula</i>	<i>Fraxinus</i>	<i>Pinus</i>	<i>Quercus</i>
PBL	0.13 <sup>***</sup>	0.13 <sup>***</sup>	0.12 <sup>***</sup>	0.08 <sup>***</sup>	0.11 <sup>***</sup>

522

523 Spearman’s rank correlations between hourly pollen concentrations and planetary  
524 boundary layer (PBL) height were positive for all taxa, indicating that higher PBL heights  
525 are generally associated with increased pollen concentrations. The strongest correlations  
526 were observed for *Betula* and *Alnus*, while *Pinus* showed the weakest relationship. All  
527 correlations were statistically significant ( $p < 0.001$ ), indicating a consistent link between  
528 boundary layer dynamics and short-term variations in pollen concentrations and  
529 highlighting the role of atmospheric mixing in pollen dispersion across different species.

530



531

532 Figure 8. Influence of wind direction on pollen concentrations by taxa.

533

534 The relationship between pollen concentrations and wind direction is presented in  
535 Fig. 8. For *Alnus*, *Betula* and *Fraxinus* the highest pollen concentrations are from the  
536 southern sector, which contributes about 25%. High contributions (20-25%) to total count  
537 is from the SE for *Betula* and *Fraxinus* and W for *Alnus*. The results are significantly  
538 different for *Pinus* and *Quercus*. *Pinus* pollen showed a clear west-east transport pattern,  
539 with the highest contributions from western (36.1%) and eastern (21%) winds, while  
540 *Quercus* pollen was mainly associated with southeastern (44.4%) and southern (27.8%)  
541 winds. Northern winds contributed minimally (<5%) to the dispersal of all taxa, with the  
542 lowest influence from NW, N and NE directions.

543

#### 544 4. Dissucion

545 Erb et al. (2025) discussed how to design measurement campaigns and mentioned that  
546 local data collection is crucial for accurate model calibration. Our study confirms that the  
547 newly developed model, trained on locally collected pollen data, outperforms the model  
548 retrained on data from a different region. However, it is important to note that the new  
549 model was also trained using fluorescence information, which could improve detection  
550 efficiency (Crouzy et al., 2025). New model more accurately capturing both the seasonal  
551 timing and the daily variability. In contrast, the previous model tends to overestimate



552 concentration magnitudes and fails to represent temporal variations with sufficient  
553 precision.

554 The enhanced detection efficiency observed in this study aligns with the study of Maya-  
555 Manzano et al. (2023) for Munich (southern Germany), who reported comparable  $R^2$   
556 values for *Quercus* and higher values for *Fraxinus*, although lower for *Betula*. Their work  
557 also highlighted the weaker correspondence between real-time monitoring devices and  
558 Hirst-type measurements, underscoring the ongoing challenges in reconciling automated  
559 and traditional methods. While Hirst-type traps remain the gold standard in aerobiology,  
560 they have inherent limitations, such as low temporal resolution and dependence on  
561 manual counting. This raises important considerations when comparing real-time data  
562 with Hirst measurements (Tummon et al., 2024).

563 In our work, the locally trained model consistently outperformed the reference model,  
564 particularly at low and medium pollen concentrations, showing enhanced sensitivity and  
565 overall predictive accuracy. Both models achieved similar performance at high  
566 concentrations, indicating reliable detection under extreme pollen loads. This indicates  
567 that if the primary goal is to issue warnings for high pollen levels, models retrained using  
568 data from other regions may still perform adequately. However, the improved sensitivity  
569 of the locally retrained model at lower concentrations is particularly important for  
570 operational air-quality monitoring and early warning systems, as it allows for more timely  
571 identification of pollen events relevant to public health. Similar challenges related to  
572 underestimation at low concentrations were also reported by Tummon et al. (2024),  
573 further supporting the need for region-specific model retraining.

574 This study provides a detailed description of the measurement campaign and its  
575 methodology. The lowest amount of pollen was collected from *Fraxinus*, which was  
576 influenced by the low number of training events and consequently, *Fraxinus* exhibited the  
577 lowest  $R^2$  among all taxa. This underscores the importance of properly extracting  
578 sufficient amounts of pollen from catkins. *Pinus* also showed a relatively low  $R^2$  compared  
579 to *Alnus*, *Betula* and *Quercus*, which is likely due to interference from morphologically  
580 similar pollen grains, such as spruce or larch (Szczepanek et al., 2017). Therefore, one  
581 possible solution could be to aggregate data within the Pinaceae group.

582 Analysis of hourly pollen percentages revealed distinct diurnal patterns consistent with  
583 daily meteorological rhythms. *Alnus* peaked in the late afternoon (16:00–18:00) as the first  
584 major pollen-releasing taxon of the season. *Betula* and *Quercus* exhibited bimodal  
585 patterns, with morning and evening peaks. In contrast, *Fraxinus* and *Pinus* maintained  
586 relatively high pollen concentrations throughout the day. These results align with previous  
587 observations in Europe, including Ščevková et al. (2015) and Toth et al. (2011), who noted  
588 daytime peaks for *Fraxinus*, *Alnus*, *Corylus* and *Pinus*, as well as afternoon and night-time  
589 peaks for *Betula* and Cupressaceae-Taxaceae. Similar bimodal patterns have been  
590 reported by Dąbrowska-Zapart et al. (2020).



591 Our findings regarding evening peaks suggest that nocturnal maxima are influenced not  
592 only by local pollen release but also by the secondary deposition of previously emitted or  
593 transported pollen (Grewling et al., 2016; Ščevková et al., 2015). For instance, *Betula* and  
594 *Fraxinus* produce small pollen grains with low settling velocities, making them prone to  
595 long-distance transport and prolonged suspension within the atmospheric boundary  
596 layer. During daytime heating, thermal convection lifts pollen grains to higher altitudes;  
597 once convection weakens in the evening, these particles gradually descend, resulting in  
598 elevated nighttime concentrations (Clot, 2001; Kasprzyk et al., 2001; Kämpylä, 1984).

599 The local urban effects may also enhance nocturnal concentrations. The heating of  
600 anthropogenic surfaces (e.g., buildings and roads) during the day and subsequent  
601 nighttime radiative cooling can modify near-surface circulation, promoting weak  
602 turbulence and the resuspension of previously settled pollen grains. Such mechanisms  
603 may partly explain the persistence of elevated evening levels, particularly under calm and  
604 dry conditions. Given the low gravitational settling velocity of these taxa, deposition from  
605 the boundary layer (~1 km) may take more than 24 hours (Ščevková et al., 2015), further  
606 supporting the hypothesis that the observed evening and nocturnal peaks reflect both  
607 delayed sedimentation and localized resuspension.

608 Night-time increases were also noted in Kluska et al. (2020), who reported that low  
609 relative humidity and calm winds favor elevated concentrations of *Betula*, *Pinus* and  
610 Poaceae pollen at night. Resuspension of previously settled pollen appears to play a  
611 minor role in our dataset, as evening conditions, characterized by higher humidity, lower  
612 temperatures and moderate wind speeds, were generally unfavorable for significant re-  
613 entrainment, which is consistent with findings of Ščevková et al. (2015).

614 Meteorological factors were key drivers of hourly pollen variability. Our findings confirm  
615 the well-known pattern of increased pollen concentrations during warm and sunny days  
616 and decreased concentrations under high humidity or rainy conditions (Malkiewicz et al.,  
617 2016; Ščevková et al. 2015; Tomczyk et al. 2025; Ziska et al., 2019). Interestingly, early-  
618 season pollen, such as that from *Alnus*, showed no significant correlation with sunlight  
619 and even a negative association with temperature. This contrasts with the findings of  
620 Borycka and Kasprzyk (2018), who reported that *Betula* did not exhibit significant  
621 correlations with meteorological variables, while *Alnus* showed strong relationships. In  
622 the present study, *Fraxinus* and *Betula* also displayed different patterns, with no  
623 consistent correlation with temperature, whereas later-season trees, such as *Pinus* and  
624 *Quercus*, exhibited positive associations with temperature. Wind was generally an  
625 important factor influencing pollen dispersal and increasing concentrations; however,  
626 this was not observed for *Pinus*. This is likely related to the morphological features of  
627 *Pinus* pollen, which has air sacs that enhance its dispersal, combined with the high pollen  
628 output of the species, making wind less critical for effective transport (Szczepek et al.,  
629 2016).



630 Early-spring taxa, *Alnus* and *Betula*, displayed strong positive correlations with air  
631 temperature and negative correlations with relative humidity, particularly between 12:00  
632 and 18:00, when concentrations typically increased. This pattern supports the hypothesis  
633 that warm and dry afternoon conditions promote pollen release, consistent with  
634 observations by Dąbrowska-Zapart et al. (2020) and Kluska et al. (2020), who also found  
635 that high temperature and solar radiation act as primary triggers of emission. For *Betula*,  
636 the most pronounced temperature effect occurred in the late afternoon and evening  
637 (14:00-22:00), coinciding with the timing of observed concentration peaks. However, it  
638 differs between months, which suggests that the phase of pollen release is likely  
639 correlated with meteorological conditions, so the early part of the pollination period in  
640 March shows different sensitivity compared to April. It is also well known that for early-  
641 flowering plant taxa, the timing of the pollen season can vary considerably from year to  
642 year (Malkiewicz et al., 2016). Interestingly, sunshine duration was crucial only in March  
643 for both taxa and practically only during the morning hours. Many studies emphasize the  
644 importance of temperature for the development of inflorescences; however, it is possible  
645 that pollen emission and flower opening are primarily triggered by sunshine duration.  
646 Favorable thermal conditions may then mainly support continued emission and the  
647 persistence of pollen in the air, which could explain why temperature becomes more  
648 influential during the later hours of the day (Malkiewicz et al., 2016; Nowosad et al., 2018;  
649 Picornell et al., 2019; Werner et al., 2021). Among all taxa, only *Betula* exhibited a  
650 correlation with wind around midday in April. Wind was previously identified as an  
651 important factor by Puc et al. (2015) and Puc (2006), whereas Tomczyk et al. (2025)  
652 reported that wind does not play a significant role. Nevertheless, it should be noted that  
653 their findings were based on daily data, while the present analysis is conducted on an  
654 hourly scale.

655 *Fraxinus* exhibited a similar dependence on temperature and sunshine duration, with  
656 maximum correlations observed between 10:00 and 16:00. It is also evident that the daily  
657 pattern differs between months: in March, temperature was the most important factor  
658 during the day and evening, while relative humidity had a stronger effect in the evening  
659 and night. In April, temperature played a key role in the morning, evening and night,  
660 whereas relative humidity was most influential at night. Kubik-Komar et al. (2018) also  
661 identified *Fraxinus* as a taxon whose pollen concentration is particularly related to  
662 temperature, noting that the timing of the season may vary depending on meteorological  
663 conditions during the first part of the year. Therefore, the observed correlations may also  
664 differ between months, depending on the prevailing weather conditions.

665 *Pinus* showed negative correlations with temperature (morning and night) and with  
666 humidity (except in the morning), which is opposite to the results presented in the overall  
667 analysis (Fig. 7), where early-pollinating taxa showed negative correlations with  
668 temperature and *Pinus* showed positive correlations. This highlights the complex nature  
669 of the relationship between pollen concentration and meteorological conditions. It



670 should be underlined that the aerodynamic properties of *Pinus* pollen allow it to remain  
671 airborne for a long time, which may explain the lack of correlation with current  
672 meteorological conditions, as this pollen could have been released earlier (Szczepanek  
673 et al., 2016).

674 *Quercus*, which flowers later in the season, was strongly responsive to temperature  
675 throughout the day, exhibiting a bimodal pollen release pattern with peaks in the morning  
676 (06:00–09:00) and evening (18:00–22:00), likely reflecting local meteorological control.  
677 Interestingly, temperature appeared to be important throughout the entire day only in  
678 April, probably because approximately 75% of the seasonal pollen amount occurs during  
679 the first two weeks of the season, as noted by Grewling et al. (2013).

680 The positive and statistically significant correlations between planetary boundary layer  
681 height and hourly pollen concentrations suggest that atmospheric mixing plays an  
682 important role in the short-term variability of pollen levels, as confirmed by Andújar-  
683 Maqueda et al. (2025). Stronger correlations observed for *Betula* and *Alnus* compared to  
684 *Pinus* may reflect differences in pollen release patterns and dispersal mechanisms. In  
685 particular, *Pinus* pollen, due to its aerodynamic shape and morphology, may be dispersed  
686 through mechanisms less directly linked to planetary boundary layer height. This is  
687 supported by the lack of a significant correlation with wind speed, suggesting that other  
688 factors, such as local turbulence or canopy-level processes, could play a more important  
689 role in its short-term variability.

690 Wind direction also played a significant role in shaping hourly pollen levels. The highest  
691 concentrations were typically linked to airflows from vegetated areas upwind of the  
692 monitoring site. This finding is consistent with Dąbrowska-Zapart et al. (2020), who also  
693 demonstrated that wind direction significantly influences short-term (hourly) variations in  
694 pollen and spore concentrations.

695 Overall, our results highlight the need to consider taxon-specific diurnal patterns,  
696 meteorological drivers and local environmental context when interpreting pollen  
697 measurements and developing predictive models. The combination of high temporal  
698 resolution monitoring and incorporation of local taxa into model training substantially  
699 improves the ability to capture real-time pollen fluctuations, peak exposure periods and  
700 species-specific variability, which are critical for accurate forecasting and public health  
701 applications.

702

## 703 **6. Conclusion**

704 Our results showed that retraining the neural network model with locally collected pollen  
705 data improves predictive accuracy for *Alnus*, *Betula*, *Fraxinus*, *Pinus* and *Quercus*,  
706 especially at low and medium pollen concentrations, compared to models trained on  
707 data from other regions. The retrained model correlates more closely with Hirst



708 measurements in terms of the start and end of the season, as well as the concentration  
709 levels and can provide valuable information for pollen information system or pollen  
710 forecasting.

711 Based on two years of automatic pollen concentration measurements, we present diurnal  
712 pollen variability, which exhibits distinct patterns depending on the taxon. People with  
713 allergies should avoid pollen peak hours. These are:

- 714 • *Alnus*: late afternoon peak (16:00-18:00)
- 715 • *Betula*: evening peak (18:00-22:00)
- 716 • *Fraxinus*: midday peak (12:00-13:00), additional moderate afternoon peaks
- 717 • *Pinus*: high levels throughout the day, morning and midday peaks (10:00)
- 718 • *Quercus*: bimodal pattern - morning (06:00-09:00) and evening (18:00-22:00)  
719 peaks

720 Temperature and low relative humidity are the main drivers of pollen release, while  
721 sunshine duration enhances emission for *Fraxinus*, *Pinus* and *Quercus*. Hourly analyses  
722 reveal that the strength of correlations between pollen concentrations and  
723 meteorological factors varies throughout the day and depends on the phase of the  
724 flowering season or month.

725 The planetary boundary layer height has only a limited direct influence on hourly pollen  
726 concentration variability, with particularly lower correlations observed for *Pinus*.

727 Wind direction affects pollen dispersal, with southern and southeastern winds  
728 contributing most, highlighting the influence of local land cover and the surroundings of  
729 the monitoring station.

730

#### 731 **Code availability**

732 Code will be made available on request.

733

#### 734 **Data availability**

735 Data will be made available on request.

736

#### 737 **Author contribution**

738 Tomczyk Szymon: Conceptualization, Methodology, Investigation, Formal analysis,  
739 Writing - Original Draft, Writing – review and editing, Visualization.



740 Małgorzata Werner: Supervision, Funding acquisition, Writing - Review & Editing,  
741 Investigation.

742 Małgorzata Malkiewicz: Supervision, Writing - Review & Editing, Investigation.

743 Karol Bubel: Writing - Review & Editing, Investigation.

744

#### 745 **Competing interests**

746 The authors declare that they have no conflict of interest.

747

#### 748 **Acknowledgement**

749 The calculation of PBL height using WRF was carried out at the Wrocław Centre for  
750 Networking and Supercomputing (<http://www.wcss.wroc.pl>), Grant No. 170.

751

#### 752 **Financial support**

753 The study was funded by the National Science Centre, Poland grants no  
754 2023/51/B/ST10/01361 and no UMO2024/53/N/ST10/01341. For the purpose of Open  
755 Access, the authors have applied a CC-BY public copyright licence to any Author  
756 Accepted Manuscript version arising from this submission.

757

758

#### 759 **7. Literature**

760 Adamov, S., Lemonis, N., Clot, B., et al. (2024). On the measurement uncertainty of Hirst-  
761 type volumetric pollen and spore samplers. *Aerobiologia*, 40, 77–91.  
762 <https://doi.org/10.1007/s10453-021-09724-5>

763 Adams-Groom, B., Selby, K., Derrett, S., Frisk, C. A., Pashley, C. H., Satchwell, J., King, D.,  
764 McKenzie, G., & Neilson, R. (2022). Pollen season trends as markers of climate change  
765 impact: *Betula*, *Quercus* and *Poaceae*. *Science of The Total Environment*, 831, 154882.  
766 <https://doi.org/10.1016/j.scitotenv.2022.154882>

767 Anderegg, W. R. L., Abatzoglou, J. T., Anderegg, L. D. L., Bielory, L., Kinney, P. L., & Ziska, L.  
768 (2021). Anthropogenic climate change is worsening North American pollen seasons.  
769 *Proceedings of the National Academy of Sciences of the United States of America*, 118(7),  
770 e2013284118. <https://doi.org/10.1073/pnas.2013284118>

771 Andújar-Maqueda, J., Ortiz-Amezcue, P., Cariñanos, P., Abril-Gago, J., De Linares, C., de  
772 Arruda Moreira, G., Bravo-Aranda, J. A., Granados-Muñoz, M. J., Alados-Arboledas, L., &



- 773 Guerrero-Rascado, J. L. (2025). The role of atmospheric boundary layer wind and  
774 turbulence on surface pollen levels. *Agricultural and Forest Meteorology*, 371, 110584.  
775 <https://doi.org/10.1016/j.agrformet.2025.110584>
- 776 Beggs, P. J., Clot, B., Sofiev, M., & Johnston, F. H. (2023). Climate change, airborne  
777 allergens, and three translational mitigation approaches. *eBioMedicine*, 93, 104478.  
778 <https://doi.org/10.1016/j.ebiom.2023.104478>
- 779 Biedermann, T., Winther, L., Till, S. J., Panzner, P., Knulst, A., & Valovirta, E. (2019). Birch  
780 pollen allergy in Europe. *Allergy*, 74, 1237–1248. <https://doi.org/10.1111/all.13758>
- 781 Borycka, K., & Kasprzyk, I. (2018). Hourly pattern of allergenic alder and birch pollen  
782 concentrations in the air: Spatial differentiation and the effect of meteorological  
783 conditions. *Atmospheric Environment*, 182, 179–192.  
784 <https://doi.org/10.1016/j.atmosenv.2018.03.048>
- 785 Buters, J., Clot, B., Galán, C., et al. (2024). Automatic detection of airborne pollen: An  
786 overview. *Aerobiologia*, 40, 13–37. <https://doi.org/10.1007/s10453-022-09750-x>
- 787 CEN/TS 16868. (2015). Ambient air. Sampling and analysis of airborne pollen grains and  
788 fungal spores for allergy networks. Volumetric Hirst method.
- 789 Clot, B. (2001). Airborne birch pollen in Neuchâtel (Switzerland): Onset, peak and daily  
790 patterns. *Aerobiologia*, 17, 25–29. <https://doi.org/10.1023/A:1007652220568>
- 791 Crouzy, B., Meurville, MP., Clot, B. *et al.* (2025). Operational pollen classification using  
792 digital holography and fluorescence. *Aerobiologia*, 41, 841–846.  
793 <https://doi.org/10.1007/s10453-025-09882-w>
- 794 D'Amato, G., Cecchi, L., Bonini, S., Nunes, C., Annesi-Maesano, I., Behrendt, H., Liccardi,  
795 G., Popov, T., & Van Cauwenberge, P. (2007). Allergenic pollen and pollen allergy in Europe.  
796 *Allergy*, 62, 976–990. <https://doi.org/10.1111/j.1398-9995.2007.01393.x>
- 797 Dąbrowska-Zapart, K., & Niedźwiedz, T. (2020). Height and hourly variations in the  
798 concentration of airborne pollen grains and fungal spores in Sosnowiec (Poland).  
799 *Alergoprofil*, 16(1), 21–23. <https://doi.org/10.24292/01.AP.161120220>
- 800 Erb, S., Graf, E., Zeder, Y., Lionetti, S., Berne, A., Clot, B., Lieberherr, G., Tummon, F.,  
801 Wullschleger, P., & Crouzy, B. (2024). Real-time pollen identification using holographic  
802 imaging and fluorescence measurements. *Atmospheric Measurement Techniques*, 17,  
803 441–451. <https://doi.org/10.5194/amt-17-441-2024>
- 804 Erb, S., Berne, A., Clot, B., et al. (2025). Pollen holographic images and light-induced  
805 fluorescence measurements at the species level. *Scientific Data*, 12, 786.  
806 <https://doi.org/10.1038/s41597-025-05139-w>



- 807 Farooq, Q., Oteros, J., & Galán, C. (2025). Advancing in the pollen frontier: A  
808 comprehensive evaluation and meta-analysis of automatic pollen monitoring systems.  
809 *Aerobiologia*, 41, 527–546. <https://doi.org/10.1007/s10453-025-09865-x>
- 810 Galán, C., Smith, M., Thibaudon, M., et al. (2014). Pollen monitoring: Minimum  
811 requirements and reproducibility of analysis. *Aerobiologia*, 30, 385–395.  
812 <https://doi.org/10.1007/s10453-014-9335-5>
- 813 Gimenez, B., Joannin, S., Pasquet, J., Beaufort, L., Gally, Y., de Garidel-Thoron, T.,  
814 Combourieu-Nebout, N., Bouby, L., Canal, S., Ivorra, S., Limier, B., Terral, J.-F., Devaux, C.,  
815 & Peyron, O. (2024). A user-friendly method to get automated pollen analysis from  
816 environmental samples. *New Phytologist*, 243, 797–810.  
817 <https://doi.org/10.1111/nph.19857>
- 818 Grewling, Ł., Jackowiak, B., & Smith, M. (2014). Variations in *Quercus* sp. pollen seasons  
819 (1996–2011) in Poznań, Poland, in relation to meteorological parameters. *Aerobiologia*,  
820 30, 149–159. <https://doi.org/10.1007/s10453-013-9313-3>
- 821 Grewling, Ł., Bogawski, P., & Smith, M. (2016). Pollen nightmare: Elevated airborne pollen  
822 levels at night. *Aerobiologia*, 32(4), 725–728. <https://doi.org/10.1007/s10453-016-9441-7>
- 823 Grewling, Ł., Ribeiro, H., Antunes, C., Apangu, G. P., Çelenk, S., et al. (2023). Outdoor  
824 airborne allergens: Characterization, behavior and monitoring in Europe. *Science of The*  
825 *Total Environment*, 905, 167042. <https://doi.org/10.1016/j.scitotenv.2023.167042>
- 826 Hirst, J. M. (1952). An automatic volumetric spore trap. *Annals of Applied Biology*, 39(2),  
827 257–265. <https://doi.org/10.1111/j.1744-7348.1952.tb00904.x>
- 828 Kasprzyk, I., Harmata, K., Myszkowska, D., et al. (2001). Diurnal variation of chosen  
829 airborne pollen at five sites in Poland. *Aerobiologia*, 17, 327–345.  
830 <https://doi.org/10.1023/A:1013078627196>
- 831 Kluska, K., Piotrowicz, K., & Kasprzyk, I. (2020). The impact of rainfall on the diurnal  
832 patterns of atmospheric pollen concentrations. *Agricultural and Forest Meteorology*, 291,  
833 108042. <https://doi.org/10.1016/j.agrformet.2020.108042>
- 834 Kubik-Komar, A., Piotrowska-Weryszko, K., Weryszko-Chmielewska, E., & Kaszewski, B.  
835 M. (2018). Analysis of *Fraxinus* pollen seasons and forecast models based on  
836 meteorological factors. *Annals of Agricultural and Environmental Medicine*, 25(2), 285–  
837 291. <https://doi.org/10.26444/aaem/80909>
- 838 Käpylä, M. (1984). Diurnal variation of tree pollen in the air in Finland. *Grana*, 23(3), 167–  
839 176. <https://doi.org/10.1080/00173138409427712>
- 840 Lake, I. R., Jones, N. R., Agnew, M., Goodess, C. M., Giorgi, F., Hamaoui-Laguel, L., et al.  
841 (2017). Climate change and future pollen allergy in Europe. *Environmental Health*  
842 *Perspectives*, 125(3), 385–391. <https://doi.org/10.1289/EHP173>



- 843 Malkiewicz, M., Drzeniecka-Osiadacz, A., & Krynicka, J. (2016). The dynamics of the  
844 Corylus, Alnus, and Betula pollen seasons in the context of climate change (SW Poland).  
845 Science of The Total Environment, 573, 740–750.  
846 <https://doi.org/10.1016/j.scitotenv.2016.08.103>
- 847 Maya-Manzano, J. M., Tummon, F., Abt, R., et al. (2023). Towards European automatic  
848 bioaerosol monitoring: Comparison of 9 automatic pollen observational instruments with  
849 classic Hirst-type traps. Science of The Total Environment, 866, 161220.  
850 <https://doi.org/10.1016/j.scitotenv.2022.161220>
- 851 MeteoSwiss. (2022). SwissPollen models [GitHub repository]. GitHub.  
852 <https://github.com/MeteoSwiss/swisspollen-models>
- 853 Nilsson, S., & Persson, S. (1981). Tree pollen spectra in the Stockholm region (Sweden),  
854 1973–1980. Grana, 20(3), 179–182. <https://doi.org/10.1080/00173138109427661>
- 855 Nowosad, J., Stach, A., Kasprzyk, I., et al. (2018). Statistical techniques for modeling of  
856 Corylus, Alnus, and Betula pollen concentration in the air. Aerobiologia, 34, 301–313.  
857 <https://doi.org/10.1007/s10453-018-9514-x>
- 858 Pacheco, S. E., Guidos-Fogelbach, G., Annesi-Maesano, I., et al. (2021). Climate change  
859 and global issues in allergy and immunology. Journal of Allergy and Clinical Immunology,  
860 148(6), 1366–1377. <https://doi.org/10.1016/j.jaci.2021.10.011>
- 861 Paudel, B., Chu, T., Chen, M., et al. (2021). Increased duration of pollen and mold  
862 exposure are linked to climate change. Scientific Reports, 11, 12816.  
863 <https://doi.org/10.1038/s41598-021-92178-z>
- 864 Picornell, A., Buters, J., Rojo, J., et al. (2019). Predicting the start, peak and end of the  
865 Betula pollen season in Bavaria, Germany. Science of The Total Environment, 690, 1299–  
866 1309. <https://doi.org/10.1016/j.scitotenv.2019.06.485>
- 867 Puc, M., Wolski, T., Camacho, I. C., Myszkowska, D., Kasprzyk, I., Grewling, Ł., et al.  
868 (2015). Fluctuation of birch (Betula L.) pollen seasons in Poland. Acta Agrobotanica,  
869 68(4). <https://doi.org/10.5586/aa.2015.041>
- 870 Puc, M. (2006). Birch pollen grains in the air of Szczecin in 2000–2004. Acta Agrobotanica,  
871 59(1). <https://doi.org/10.5586/aa.2006.034>
- 872 Rapiejko, P., Stankiewicz, W., & Szczygielski, K., Jurkiewicz, D. (2007). Threshold pollen  
873 concentration required to trigger allergic symptoms. Otolaryngologia Polska, 61(4), 591–  
874 594. [https://doi.org/10.1016/S0030-6657\(07\)70491-2](https://doi.org/10.1016/S0030-6657(07)70491-2)
- 875 Rodríguez-Rajo, F. J., Fdez-Sevilla, D., Stach, A., et al. (2010). Assessment between pollen  
876 seasons in areas with different urbanization level related to local vegetation sources and  
877 differences in allergen exposure. Aerobiologia, 26, 1–14. <https://doi.org/10.1007/s10453-009-9138-2>  
878



- 879 Rojo, J., Cervigón, P., Ferencova, Z., et al. (2024). Assessment of environmental risk areas  
880 based on airborne pollen patterns as a response to land use and land cover distribution.  
881 *Environmental Pollution*, 344, 123385. <https://doi.org/10.1016/j.envpol.2024.123385>
- 882 Sauvageat, E., Zeder, Y., Auderset, K., et al. (2020). Real-time pollen monitoring using  
883 digital holography. *Atmospheric Measurement Techniques*, 13, 1539–1550.  
884 <https://doi.org/10.5194/amt-13-1539-2020>
- 885 Shamrat, F. M. J., Idris, M. Y. I., Zhou, X., et al. (2024). PollenNet: A novel architecture for  
886 high precision pollen grain classification through deep learning and explainable AI.  
887 *Heliyon*, 10(19), e38596. <https://doi.org/10.1016/j.heliyon.2024.e38596>
- 888 Skamarock, W. C., Klemp, J. B., Dudhia, J., et al. (2021). A description of the Advanced  
889 Research WRF Model Version 4.3. NCAR/TN-556+STR. Boulder, Colorado, USA.  
890 <https://doi.org/10.5065/1dfh-6p97>
- 891 Szczepanek, K., Myszkowska, D., Worobiec, E., et al. (2017). The long-range transport of  
892 Pinaceae pollen: An example in Kraków (southern Poland). *Aerobiologia*, 33(1), 109–125.  
893 <https://doi.org/10.1007/s10453-016-9454-2>
- 894 Ščevková, J., Dušička, J., Mičieta, K., et al. (2015). Diurnal variation in airborne pollen  
895 concentration of six allergenic tree taxa and its relationship with meteorological  
896 parameters. *Aerobiologia*, 31, 457–468. <https://doi.org/10.1007/s10453-015-9379-1>
- 897 Tomczyk, S., Werner, M., Malkiewicz, M., et al. (2025). Influence of meteorological  
898 conditions and climate on pollen season of the early-flowering woody taxa in Poland,  
899 Central Europe. *International Journal of Biometeorology*. <https://doi.org/10.1007/s00484-900-025-02995-4>
- 901 Toth, I., Peternel, R., Srnc, L., & Vojniković, B. (2011). Diurnal variation in airborne pollen  
902 concentrations of the selected taxa in Zagreb, Croatia. *Collegium Antropologicum*, 35,  
903 43–50.
- 904 Triviño, M. M., Maya-Manzano, J. M., Tummon, F., et al. (2023). Variability between Hirst-  
905 type pollen traps is reduced by resistance-free flow adjustment. *Aerobiologia*, 39, 257–  
906 273. <https://doi.org/10.1007/s10453-023-09790-x>
- 907 Tummon, F., Adamov, S., Clot, B., et al. (2024). A first evaluation of multiple automatic  
908 pollen monitors run in parallel. *Aerobiologia*, 40, 93–108. <https://doi.org/10.1007/s10453-909-021-09729-0>
- 910 Werner, M., Guzikowski, J., Kryza, M., et al. (2021). Extension of WRF-Chem for birch  
911 pollen modelling—a case study for Poland. *International Journal of Biometeorology*, 65,  
912 513–526. <https://doi.org/10.1007/s00484-020-02045-1>
- 913 World Allergy Organization. (2013). WAO White Book on Allergy: Update 2013. Milwaukee,  
914 WI: World Allergy Organization.

<https://doi.org/10.5194/egusphere-2025-5874>

Preprint. Discussion started: 30 March 2026

© Author(s) 2026. CC BY 4.0 License.



915 Ziska, L. H., Makra, L., Harry, S. K., Bruffaerts, N., Hendrickx, M., et al. (2019).  
916 Temperature-related changes in airborne allergenic pollen abundance and seasonality  
917 across the Northern Hemisphere: A retrospective data analysis. *Lancet Planetary Health*,  
918 3(3), 124–131. [https://doi.org/10.1016/S2542-5196\(19\)30031-7](https://doi.org/10.1016/S2542-5196(19)30031-7)